A SIMULATION FRAMEWORK FOR AGRIVOLTAIC SYSTEMS: DESIGN AND PERFORMANCE EVALUATION

Andrea Ademollo[1]*, Lorenzo Ferretti[2], Niccolò Ulivi[1], Francesco Serafini[2], Carlo Carcasci[1], Cesare Pacini[2]

[1]Università degli Studi di Firenze, Department of Industrial Engineering - DIEF, Via di Santa Marta 3, 50139 Firenze, Italy

[2]Università degli Studi di Firenze, Department of Agricultural, Food, Environmental and Forestry Science and Technology - DAGRI, Piazzale delle Cascine 18, 50144 Firenze, Italy

*Corresponding Author: andrea.ademollo@unifi.it

ABSTRACT

The rising demand for renewable energy has led to an increased deployment of ground-mounted Photovoltaic (PV) systems on arable land, often triggering competition between food production and energy generation. Advanced Agrivoltaic (AV) systems offer a promising solution by allowing crop cultivation underneath and between rows of elevated PV panels. This paper presents the design and performance evaluation of an advanced AV system focused on potato cultivation in the Follonica area (Tuscany, Italy). A modeling approach was used to quantify both solar energy generation and the impact of partial shading on the crop. Two-dimensional simulations of ground irradiance were carried out to assess the shading footprint from tilted PV arrays throughout the day. Subsequently, a crop-growth model was employed to estimate biomass production under these varying light conditions. Results include assessments of shading distribution, potato yield, and agronomic feasibility. The analysis indicates that while shading can reduce incident radiation in certain parts of the field, it also mitigates water stress under high-evapotranspiration conditions. In the selected layout, yields in specific shaded corridors were comparable or even 10% higher than those grown under full sunlight, demonstrating the potential synergy between renewable energy production and crop cultivation.

1 INTRODUCTION

Global efforts to meet escalating energy demands through renewable sources often collide with the imperative to safeguard arable land for food production. Traditional ground-mounted Photovoltaic (PV) farms can occupy significant agricultural space, potentially displacing crop cultivation and contributing to farmland abandonment (Zavalloni *et al.*, 2021). Coupled with the risks posed by climate change, such as increased water scarcity (Ingrao *et al.*, 2023), the quest to balance energy generation and food production has assumed growing importance. Agrivoltaic (AV) systems provide a means of reconciling these objectives by integrating agriculture with solar power, thereby reducing land-use conflicts (Mamun *et al.*, 2022).
Several studies have underscored the dual benefits of AV. According to Elamri *et al*. (2018), the strategic positioning of PV panels may decrease irrigation requirements, while Barron-Gafford *et al*. (2019) observed that partial shading can mitigate water stress and moderate daily maximum temperatures, particularly in drought-prone areas. Amaducci *et al*. (2018) further highlighted that these benefits are not uniform across locations; site-specific parameters such as crop type, climate, and panel configuration ultimately govern the system's overall performance (Tan *et al*., 2025).
Potatoes (Solanum tuberosum L.) have emerged as a promising crop candidate for AV installations due to their moderate tolerance to shade and sensitivity to water shortages (Widmer *et al*., 2024). Empirical data show that tuber yields can be either reduced, increased, or remain unchanged relative to open-field scenarios, depending on whether the beneficial effects of lower evapotranspiration outweigh the photosynthetic losses caused by reduced solar radiation (Weselek *et al*., 2021). Particularly in the

Mediterranean region—where rising temperatures and water scarcity threaten crop productivity (Pulighe *et al*., 2024)—the interplay between shading-induced water conservation and potential yield penalties is a subject of heightened interest.
In Italy, interest in AV is growing due to the country's commitment to expanding solar capacity while preserving its agricultural heritage. Follonica (Tuscany) offers suitable conditions for such a study, characterized by relatively high solar irradiation and a farming tradition in vegetable crops, including potatoes.

1.1 Aim and novelty of the study

This work aims to (i) design an AV layout for potato cultivation that satisfies national guidelines (elevated panels, limited land coverage), (ii) simulate shading patterns using PVGIS-based data for the Follonica site, and (iii) estimate potato yields under those conditions.
Overall, this study contributes to the emerging body of knowledge on AV systems by providing a methodology to assess the potential trade-offs and synergies between solar energy production and potato cropping. The findings presented can guide practitioners and policymakers in developing sustainable layouts that minimize conflicts over land while enhancing food production and clean energy generation.

2 MATERIALS AND METHODS

The methodological framework consists of two major components: (i) a shading and radiation-transposition model that calculates ground-level irradiance beneath the PV modules using hourly meteorological inputs; and (ii) a crop-growth model, which uses daily meteorological inputs and the computed radiation data to simulate potato biomass evolution under partial shade, as represented in Figure 1.

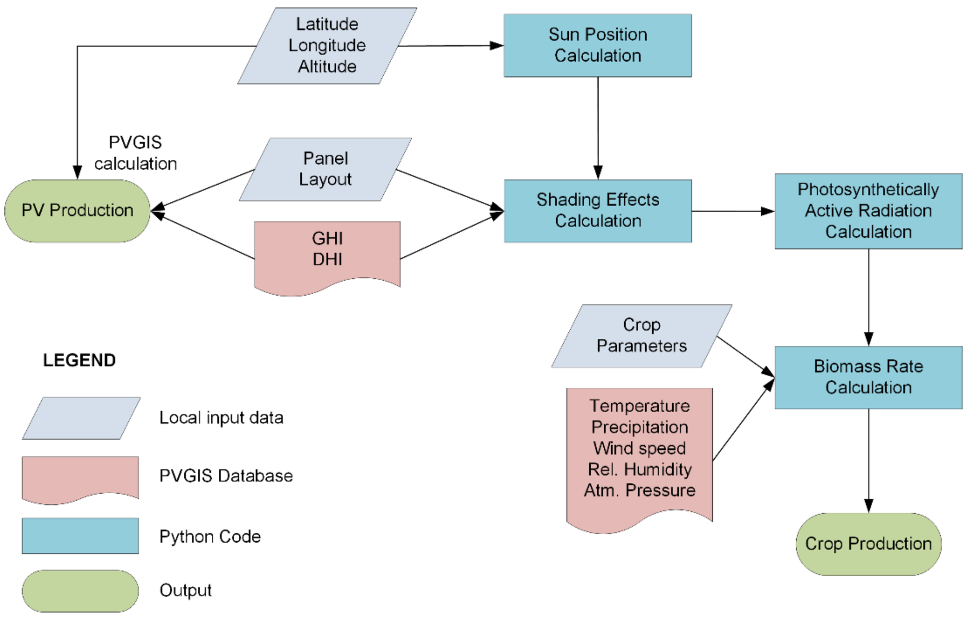

Figure 1: Modeling Workflow for AV System Simulation

Data for solar radiation and weather variables (temperature, relative humidity, etc.) were obtained from PVGIS for the location of Follonica. Below, the approach for shading calculations and the subsequent integration of those results into the crop model is detailed.

2.1 Shading Calculations and Ground Irradiance

A precise assessment of light availability beneath the PV array is fundamental to understanding potential gains or losses in crop productivity. The present study employs a geometric approach under the assumption of parallel solar rays (Figure 2). At any given time step, the sun's position is defined by its azimuth (γ_s) and zenith (θ_z) angles. Let l and w be the length and width of each PV panel, tilted at an angle β and mounted at a height h above the ground. To locate the panel's four corners, we adopt a local 3D reference frame (x, y, z) where z is vertical, as given in Equation (1).

$$\begin{cases} P_j = (x_j, y_j, z_j), \quad j \in \{A, B, C, D\} \\ z_j = h + \frac{w}{2} \times \sin\beta \quad j \in \{A, B\} \\ z_j = h - \frac{w}{2} \times \sin\beta \quad j \in \{C, D\} \end{cases} \tag{1}$$

Once each corner's position is established, the projection of that corner's shadow onto the ground is found by extending a line from (x_j,y_j,z_j) in the opposite direction of the incoming solar rays. The horizontal distance from the panel to its ground shadow can be written as in Equation (2).

$$L_j = \frac{z_j}{\tan(90 - \theta_z)} \tag{2}$$

so that the coordinates of the shadowed point P_j' can be expressed as in Equation (3).

$$P_j' = (x_j + L_j \times \sin\gamma_s, y_j + L_j \times \cos\gamma_s, 0) \tag{3}$$

The four corners project to A', B', C' and D', forming a quadrilateral on the ground. The geometric approach described above allows a fine-grained assessment of how each PV panel casts its shadow. When the tilt angle β = 0°, the shadow region remains essentially congruent to the rectangular module shape but shifts horizontally with the sun's azimuth. Conversely, as shown in Figure 2, for nonzero tilt (β > 0°), the module's upper corners rise, increasing its vertical profile and casting a shadow larger than its physical footprint, while the lower vertices project closer to the base, further expanding the shaded area. This effect is especially pronounced when the solar zenith angle is large, producing elongated shadows across the field.
At each time step, panel geometry is projected onto the ground via Eqs. (1)–(3). The field is discretized into cells, and each cell's center is tested for inclusion within the panel's shadow quadrilateral. In agreement with Valle *et al*. (2017), cells inside the shaded region receive only diffuse irradiance, while cells outside receive both direct beam and diffuse components. Global Horizontal Irradiance (GHI) and Diffuse Horizontal Irradiance (DHI) are sourced from PVGIS (European Commission, 2023). To convert incoming radiation to Photosynthetically Active Radiation (PAR) [W/m²], a constant ratio of 0.48 is applied—i.e., PAR = 0.48 × GHI for unshaded and 0.48 × DHI for shaded cells (McCree, 1966; Foyo-Moreno *et al.*, 2017). Though variable, this ratio typically ranges from 0.40÷0.50 (Tsubo and Walker, 2005; Ferrera-Cobos *et al.*, 2020), making 0.48 a sound choice for AV scenarios.

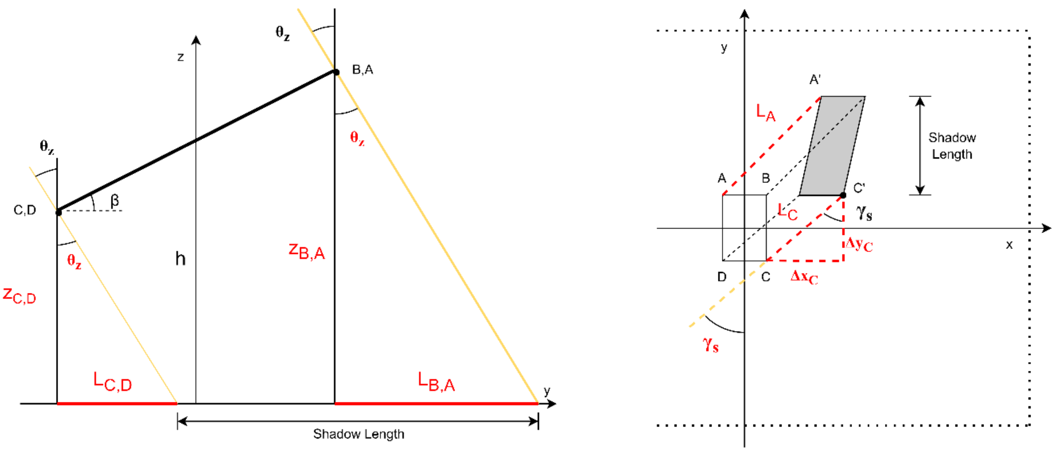

Figure 2: Shading modelling approach

By repeating these geometric shadow computations every 5 minutes throughout the potato-growing season, a high-resolution spatiotemporal PAR map is created, quantifying the extent and duration of shading experienced at any point in the field.
Although multiple transposition formulas exist to estimate tilted-plane irradiance, the authors chose to rely on PVGIS database's built-in functions for PV electricity output computation.

2.2 Crop Growth Model

To capture the influence of partial shading on potato yield, the Simple Crop model has been employed by the Monteith approach (Monteith, 1965; Zhao *et al*., 2019). Here, daily biomass accumulation in each grid cell depends primarily on the fraction of PAR intercepted by the crop canopy, the Radiation Use Efficiency (RUE), and a series of stress factors reflecting temperature extremes and water availability (Amaducci *et al*., 2018; Widmer *et al*., 2024).
The crop lifecycle is divided into three main phases—establishment, peak growth, and senescence—spanning from sowing (approximately early spring) to maturity (mid-summer). Although the exact timing can vary by cultivar and local weather, potatoes in coastal Tuscany generally follow a late-winter or early-spring planting schedule to avoid the hottest months.
Formally, if B(t) [g/m^2] is the cumulative biomass at day t, then daily growth ΔB(t) [g/m^{2}day] can be expressed as in Equation (4).

$$\Delta B(t) = RUE \times PAR(t) \times fSolar(t) \times fCO_2(t) \times ftemp(t) \times min[fheat(t), fwater(t)] \quad (4)$$

Where RUE is the crop-specific radiation use efficiency, relating absorbed PAR to biomass production [g/MJ], PAR(t) is the photosynthetically active radiation [MJ/m^2] available to the crop on day t, derived from the shading model described earlier. fSolar(t) ∈ [0,0.95] is the fraction of incoming PAR that the canopy intercepts, which evolves with leaf area development and declines during senescence. $fCO_2(t)$ [>1], ftemp(t) ∈ [0,1], fheat(t) ∈ [0,1] and fwater(t) ∈ [0,1] represent respectively the influence of atmospheric CO_2 concentration, daily mean temperature, daily maximum temperature, and available soil water on biomass accumulation and they are all dimensionless.
Potato phenology is tracked using a "Growing Degree-Day" (GDD) scheme. Starting from sowing (t=0), the sum of daily temperatures above a base threshold T_{base} is accumulated. Once the thermal requirement (T_{sum}) is reached (i.e., GDD(t) reaches T_{sum}) the crop is considered physiologically mature, marking the completion of its life cycle and the cessation of biomass accumulation, as in Equation (5). However, in commercial agricultural practice, harvest often occurs before physiological maturity, as market-driven criteria (e.g., tuber size) dictate the actual harvest timing. This approach aligns with widely used agricultural models in which phenology is temperature-driven (Ritchie *et al*.,1985).

$$GDD(t) = \sum_{\tau=1}^{t} [max(T_{mean}(\tau) - T_{base}, 0)] \quad (5)$$

Where $T_{mean}(\tau)$ is the mean daily temperature on day τ.
The fraction of intercepted PAR, fSolar(t), increases as the canopy expands. Early in the season, when leaf area is limited, the plant captures only a fraction of incoming light—even if the cell is unshaded. As thermal time progresses, the leaf area grows, driving up fSolar(t) until a maximum (often reaching 0.95). During senescence, leaf area recedes, reducing intercepted PAR.
The parameters used in this model represent the thermal times for the canopy to intercept 50% of incoming light during growth (I_{50A}) and the decline to 50% at maturity (I_{50B}), respectively (Ross, J., 2012). Shading from the PV modules can exacerbate or mitigate local water-stress effects, influencing how quickly the canopy reaches its senescence threshold (i.e., I_{50B}).
The temperature-related terms in the growth model can be separated into two factors, ftemp and fheat. The first, ftemp, captures how daily temperatures mean compare to an optimum value (T_{opt}=22°C) for vegetative and tuber growth. If the mean temperature falls below this optimum, the growth rate is reduced accordingly (Ritchie *et al*.,1985). Meanwhile, fheat accounts for high-temperature stress triggered by elevated daily maxima (T_{heat}=34°C). Whenever maximum temperatures exceed this threshold, the crop begins to suffer from heat stress, curtailing biomass accumulation on those days (Asseng *et al*., 2011). In cooler periods, these two factors create an optimal temperature range for

growth indicating negligible temperature stress while in heatwaves or colder spells, they drop, signaling a more pronounced negative impact on growth.

A separate component, fwater, governs the effects of insufficient soil moisture on photosynthesis. Daily precipitation and irrigation add water to the root zone, while crop transpiration and drainage reduce it. When transpiration differs from evapotranspiration, fwater decreases proportionally, diminishing the growth rate. Under partial shading, however, evapotranspiration is reduced, which can ease water stress and boost fwater (Woli *et al*., 2012). This interplay between light interception and water conservation is one of the core rationales for AV systems in regions prone to drought or heat extremes.

Final tuber yield [t/ha] is obtained by multiplying the total shoot biomass at maturity by the Harvest Index (HI), a factor that converts biomass into yield. Following the approach in Hsiao *et al*. (2009), it is assumed a cultivar-specific HI=0.8. Because the shading distribution is spatially heterogeneous, each grid cell accumulates biomass at a slightly different rate. Summation or averaging across all cells in the 1 ha domain yields the total and mean yield for the AV field.

In essence, the model translates localized shading dynamics—driven by PV geometry and solar position—into site-specific estimates of crop growth. This, in turn, provides a framework to identify regions under the panels where shading may reduce yields and to assess whether any gains from lowered evapotranspiration can counterbalance the decrease in direct radiation.

3 CASE STUDY

A one-hectare site in Follonica, Tuscany (Italy), was selected as the setting for this study. The location benefits from ample solar irradiation, making it attractive for PV deployment, while local conditions also support potato farming in late winter and early spring. Meteorological data—specifically hourly values for GHI, DHI temperature, humidity, wind speed—were obtained from PVGIS platform for the precise coordinates of the field while precipitations were obtained from Renewable Ninja (Renewable Ninja, 2023) database as in PVGIS they are not available.

A simple AV arrangement was considered to balance accessibility for conventional farm machinery and sufficient spacing to limit land coverage. The fixed-PV modules are raised 3 m above ground level and tilted at β=30° to maximize annual PV energy production in Follonica (1350 kWh/kW). Each module measures 2 m by 1 m, with a nominal capacity of 400 W, corresponding to widely available commercial specifications (Alibaba, 2023). The modules are organized in rows of 20 units, with a 5 m spacing between each row ensuring that the projected area of the PV panels remains below 40% of the field coherently with national AV guidelines (MiTE *et al*., 2023). This configuration allows for the installation of 100 rows per hectare, resulting in a total installed capacity of approximately 0.8 MW. This represents about 80% of the conventional ground-mounted PV benchmark of 1 MW/ha obtaining a design compliant with national AV guidelines, which also require that the system's specific electrical production to exceed 60% of the standard reference PV farm.

The layout of the study area is illustrated in Figure 3.

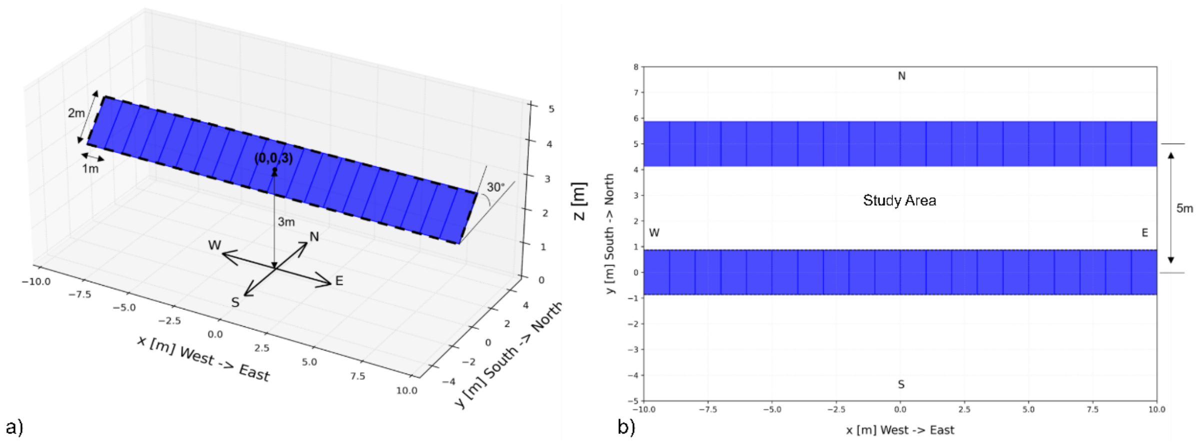

Figure 3: Case study layout; a) 3D view, b) Top view

In this layout potato plants are cultivated in rows running parallel to the PV rows, ensuring that farm machinery can pass beneath or between the elevated modules.
Table 1 provides the main input data used in the model. Crop data are retrieved from Zhao *et al*. (2019).

Table 1: Main input data

Weather data	**Symbol**	**Value**	**Unit (SI)**
Temperature	T	Hourly Serie	°C
Relative Humidity	RH	Hourly Serie	%
Global Horizontal Irradiance	GHI	Hourly Serie	W / m^2
Diffuse Horizontal Irradiance	DHI	Hourly Serie	W / m^2
Atmospheric Pressure	-	Hourly Serie	kPa
Precipitation	P	Hourly Serie	mm
Wind Speed	u	Hourly Serie	m / s
PV field data	**Symbol**	**Value**	**Unit (SI)**
Module Length	l	1	m
Module Width	w	2	m
Panel Height	h	3	m
Panel Tilt	β	30	°
Panel Azimuth	γ	0 (South)	°
Crop data	**Symbol**	**Value**	**Unit (SI)**
Thermal time for maturity	T_{sum}	2700	°C·day
Harvest Index	HI	0.8	-
Thermal time for 50% light interception (growth)	I_{50A}	690	°C·day
Thermal time for 50% light interception (senescence)	I_{50B}	400	°C·day
Base temperature for biomass growth	T_{base}	4	°C
Optimal biomass growth temperature	T_{opt}	22	°C
Heat stress threshold temperature	T_{heat}	34	°C
Radiation Use Efficiency	RUE	1.30	g / MJ

The overall objective is to analyze how partial shading—automatically generated by the tilted panels through the day—affects net biomass accumulation relative to unshaded (baseline) conditions.

4 RESULTS

An AV system was simulated for a 1 ha site in Follonica (Tuscany, Italy). The configuration consists of a fixed PV array (30° tilt) with 5 m row spacing and 3 m ground clearance. This design enables standard agricultural machinery to operate underneath the panels and is compatible with the regional directives for accessing Italian incentives (Mite, 2023). Potatoes are grown in 0.5 m rows, with sowing in early spring (March). Technical PV and potato parameters as well as meteorological data are outlined in Table 1.

4.1 Shading patterns

The first set of results focuses on Figure 4, which illustrates hourly-summed shading distributions on two clear-sky days in March and July, over a 20 m × 10 m segment of the field. Although each row in the AV system comprises multiple modules in series, this snippet isolates the influence of a single tilted module (2 m × 1 m, 3 m above the ground) to highlight how shadows propagate and overlap nearby, revealing the spatial heterogeneity of sunlight beneath the panels. Since each panel in Figure 4 shows the cumulative irradiance over the preceding hour, the shadows appear more diffused than they would at an instantaneous time point.

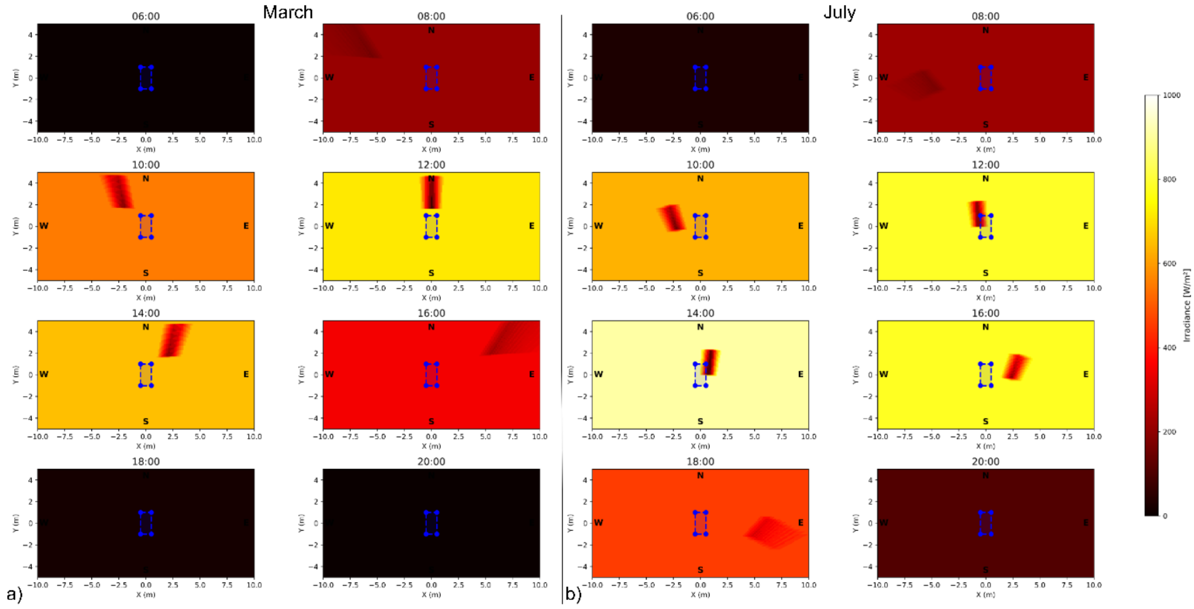

Figure 4: Hourly Ground-Level Solar Irradiance on a clear-sky day: a) March b) July

- Early Morning (06:00÷08:00): In March, when the sun rises with a relatively large zenith angle, the top edge of the module casts an elongated shadow extending north of the panel's lower edge. This shadow may reach 6÷8 m beyond the module footprint, depending on the sun's azimuth. By contrast, In July, the sun rises earlier and more to the northeast, causing the shade to fall on the southwestern quadrant.
- Midday (12:00÷14:00): Around solar noon, shading contracts closer to the panel in both months. Nonetheless, the tilt angle (30°) still causes the top corners to produce a shadow larger than the module's physical size. In March, a more pronounced solar zenith angle (i.e., a lower sun path) stretches the shade as far as 3 m north of the panel's lower edge. In July, the overall footprint is smaller and offset southward, starting roughly 0.9 m from the module's lower border, a consequence of the sun's higher altitude.
- Late Afternoon (16:00÷18:00): By late day in March, the sun's trajectory to the southwest elongates the shadow northeast. In contrast, in July, the sun sets more to the northwest, shifting the shaded area to the field's southeastern region.

Overall, Figure 4 shows that under clear-sky conditions, peak irradiance values reach approximately 930 W/m² at 13:00 in July, while in March, the midday peak is about 700 W/m². Additionally, the height difference between the upper and lower edges of the tilted panels causes shadows to extend beyond the panel boundaries, particularly at high solar zenith angles.

To further characterize the spatial distribution of radiation across the main crop-growing period, Figure 5 aggregates monthly totals of ground-level irradiation from March (crop sowing) through August (crop maturity), again focusing on a 20 m × 10 m subsection. Each pixel in this map represents the cumulative energy (kWh/m²) reaching that specific patch of soil over the given month.
As illustrated in Figure 5, the maximum monthly radiation varies significantly from one month to another, ranging from a minimum of 106 kWh/m² in March to a maximum of 225 kWh/m² in July. These simulations indicate that the module's shadow has the potential to reduce ground-level radiation by up to 15% in localized areas compared to unshaded fields. Notably, the area just north of the module center experiences consistently lower direct radiation during midday—when the sun is high—because the panels intercept a substantial portion of the direct beam. Consequently, the region north of the module relies more heavily on diffuse radiation, thereby weakening total GHI. Although higher solar

elevations in summer shrink the shaded footprint relative to early spring, shading persists in select areas directly beneath or adjacent to the panel edges.

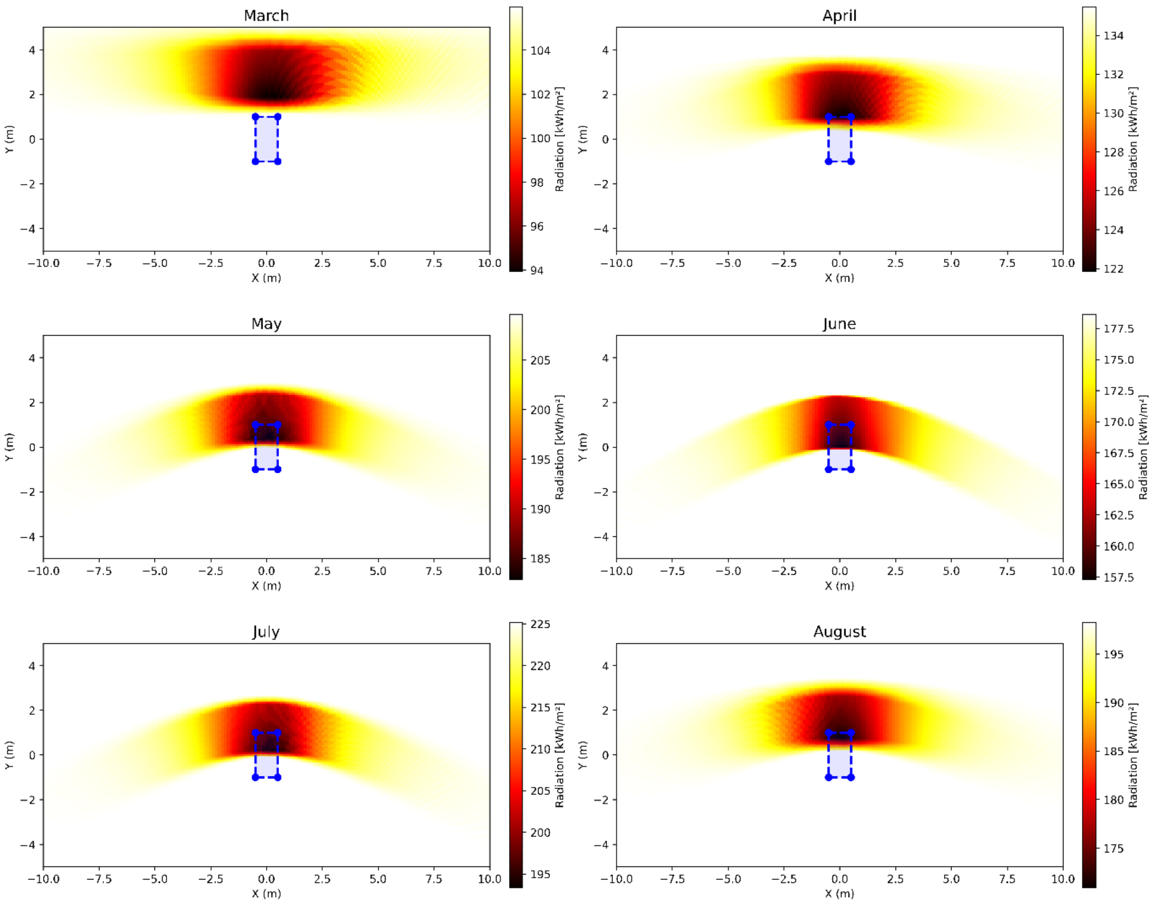

Figure 5: Seasonal Variations in Ground-Level Solar Radiation: Monthly totals from March to August

When considering the cumulative effect of a full row of 20 modules, these individual shading patterns overlap. In certain locations, the annual GHI may drop by as much as 50% compared to a scenario without any panels. These findings underscore the importance of precise shading models when evaluating AV systems.

4.2 AV performance: Biomass growth

After establishing the spatiotemporal shading patterns, and consequently the spatiotemporal PAR map (Section 2.1), the next step is to simulate potato biomass accumulation under partial shade. The adopted crop model (Section 2.2) computes biomass daily increments depending on PAR, RUE, and stress factors primarily linked to water availability. Figure 6a shows the annual PAR (accumulated from sowing in early March to physiological maturity in August) across a representative 20 m × 10 m section of the field that includes 20 adjacent PV modules. On the same spatial domain, Figure 6b displays the corresponding final potato biomass at harvest and Figure 6c depicts daily biomass accumulation throughout the year for the four represented points.

Two general observations emerge from these maps. The first one is that the impact of shading is Non-Linear as areas receiving consistently lower PAR (due to frequent or deep shadows) exhibit lower biomass but not always in direct proportion to lost radiation (Figure 6b). In locations subject to mild or intermittent shade, the decrease in direct sunlight can be partly compensated by reduced evapotranspiration, thus lowering water stress. The second one is that growth patches are heterogeneous, in fact lightly shaded cells maintain near-maximal growth rates and ultimately produce yields close to open-field scenarios while zones directly beneath modules for extended midday hours can show biomass reductions in the range of 30÷50%, depending on the intensity and duration of shade (Figure 6c).

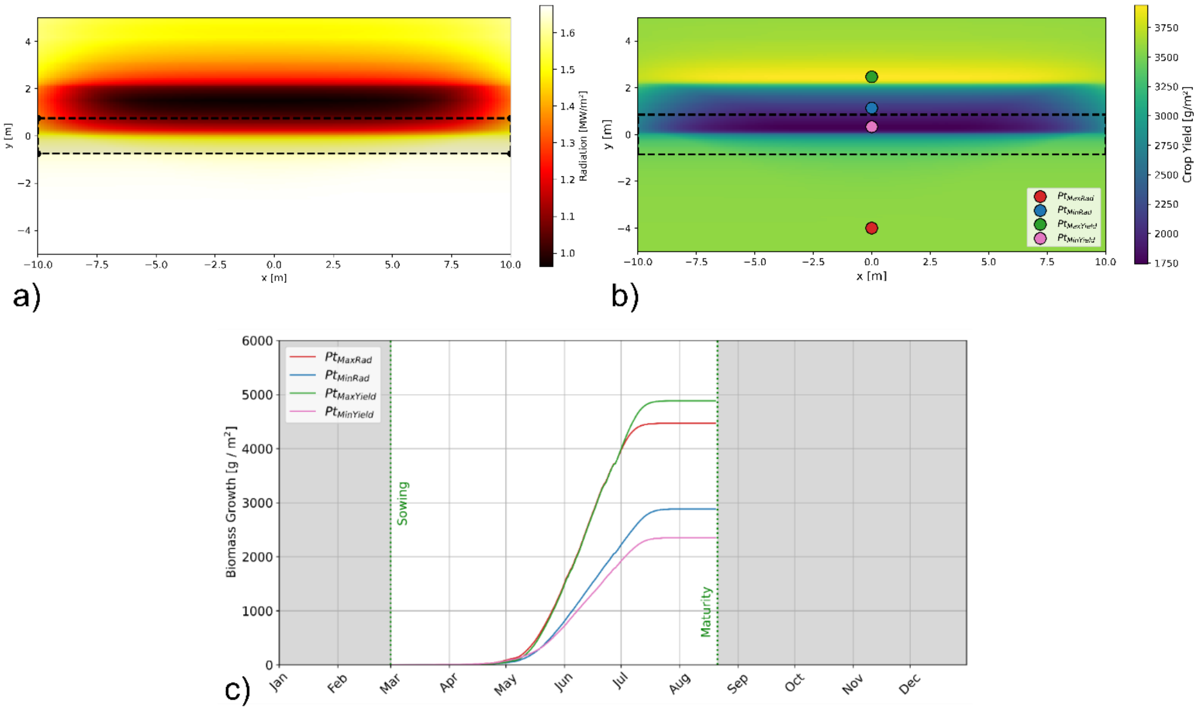

Figure 6: Spatial distribution of annual PAR (a), final crop yield (b), and daily biomass accumulation (c) across a 20 m × 10 m field section with 20 PV modules. Points represent maximum PAR (Pt_{MaxRad}), minimum PAR (Pt_{MinRad}), maximum yield ($Pt_{MaxYield}$), and minimum yield ($Pt_{MinYield}$)

To analyze localized effects in more detail, four representative points were selected, each corresponding to a different balance between radiation availability and water-stress mitigation. As schematically indicated in Figure 6b, each point exhibits a unique balance of light availability, evaporative demand, and resulting potato biomass.

- Pt_{MaxRad}: y=-4 (100% biomass, 100% PAR). Figure 7a. Located in an unshaded region about 4 m south of the PV array, this point serves as a baseline (no-panel) benchmark. Although it benefits from maximum cumulative PAR, the model detects mild yet persistent water stress as early as March, when the canopy is still small, and evaporation rates are high. In April and early May, the crop expands rapidly, with fSsolar rising to 0.8 and biomass accumulating swiftly. By mid-May to late June, near-maximum PAR interception (fSolar~0.95) fuels strong growth, but water shortages can reduce daily gains by up to one-third (fwater~0.67). Around mid-July, repeated water deficits speed up senescence and yields plateau at 100%. Overall, despite abundant sunshine, unchecked water stress shortens the most productive growth window. Physiological maturity is reached on August 24th, but the plateau indicates that commercial maturity occurs in mid-July, confirming that Desireé potato harvest takes place approximately 120 days after planting (Waddington, 2024).
- $Pt_{MaxYield}$: y=2.5 (110% biomass, 78% PAR). Figure 7b. Receiving about 23% less total PAR than Pt_{MaxRad}, this partially shaded zone achieves a 10% yield increment, demonstrating the importance of water stress effects. In March and April, moderate shading keeps soil moisture at near-optimal levels (fwater~1.0) differently from Pt_{MaxRad}, reducing early water deficits. As the canopy reaches peak coverage in May and June, the previously slower accumulation of water stress prolongs its prime growth phase by roughly 6 days (fSolar~0.95 for 6 more days) compared to the unshaded reference (Pt_{MaxRad}). This extended period of efficient photosynthesis fully compensates for the reduction in PAR, ultimately yielding about 110% of the baseline.

This result is in line with Badr *et al.* (2022) who highlighted that potato yield is considerably affected by early water deficit compared to late water deficit.

- $Pt_{MinYield}$: y=0.3 (49% biomass, 56% PAR). Figure 7c. Combining suboptimal radiation timing with early-season water stress, this location experiences the lowest overall yield. Although the PAR is not minimal, the crop cannot effectively use the incoming light in March and April because temperatures are still relatively low, and canopy interception is modest. As water deficits emerge prematurely, mid-season shading during May–June further hinders photosynthesis when the crop most needs high light availability. By harvest in mid-July, yields settle at about 49% of the reference, highlighting how ill-timed shade and water stress can severely limit growth potential.
- Pt_{MinRad}: y=1.1 (59% biomass, 46% PAR). Figure 7d. Despite registering the lowest cumulative PAR (46%), this point finishes with a yield (59%) exceeding $Pt_{MinYield}$. During March–early April, the canopy is too small to exploit greater light inputs, so the intense shade prevents excessive water loss and maintains higher fwater. Even though shading remains significant into May–June, the crop avoids the most damaging early water deficits. As a result, final yield is marginally higher than at $Pt_{MinYield}$, underscoring that the balance between light and moisture can be more critical than absolute levels of PAR alone.

When these cell-level results are summed for the entire one-hectare field, the simulation yields a final average production of approximately (31.4 t/ha — less than 35.6 t/ha) obtained in the absence of panels, which aligns with typical potato yields in Central Italy regions like Tuscany (ISMEA, 2008). This difference corresponds to a 12% decrease under the chosen layout (30° tilt, 5 m row spacing). In some sections near or just north of each module, reductions of 30÷50 % arise in an approximately 2.2 m band extending from the panel center (y=0÷2.2 m). Within the narrow corridor of y=2.2÷2.5 m, yields transition from about 70 % to 100 % of the unshaded benchmark, while the zone spanning y=2.5÷4.8 m can reach up to 110 % due to mitigated water stress. These variations create a mosaic of crop performance, where high-shade regions lose substantial sunlight during the critical growth window of May–June and suffer lower biomass accumulation, whereas partial-shade corridors maintain more stable water availability, occasionally surpassing the yield of fully sunlight areas.

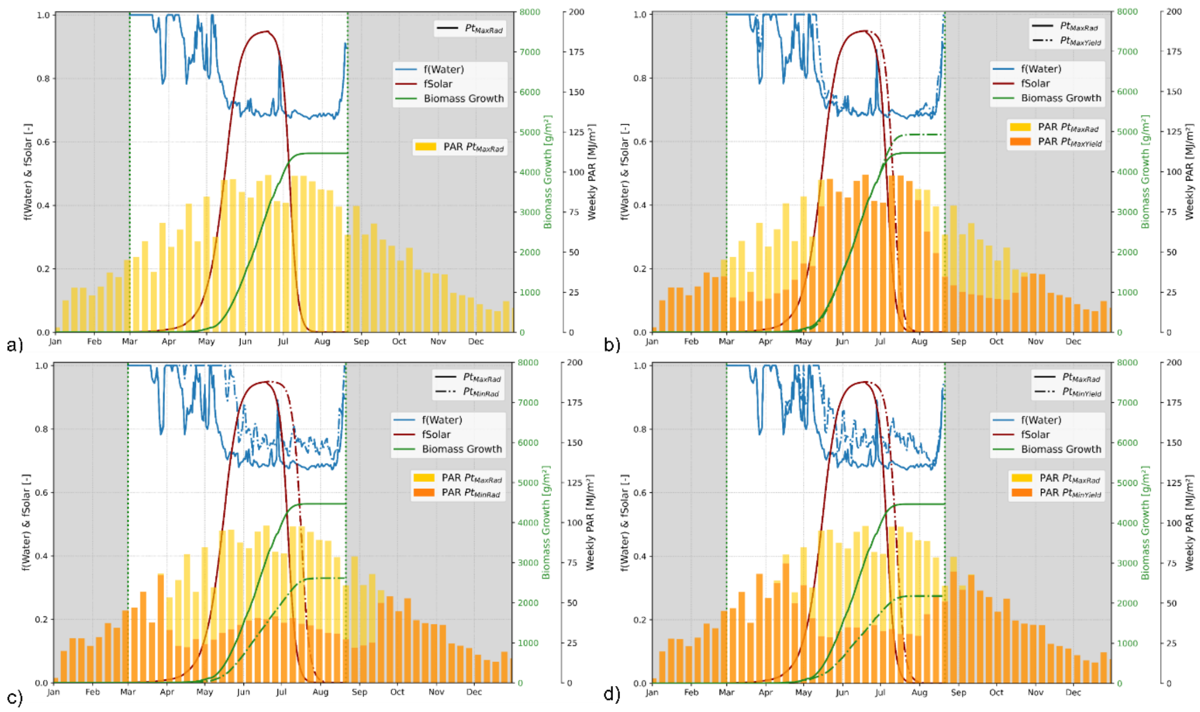

Figure 7: Daily biomass accumulation in four representative points capturing PAR, fSolar and fwater different trends: (a) Pt_{MaxRad}, (b) $Pt_{MaxYield}$, (c) $Pt_{MinYield}$, (d) Pt_{MinRad}.

5 CONCLUSIONS

- Shading Footprint: Elevated, tilted modules cast elongated shadows that vary daily and seasonally. Consequently, the photosynthetically active radiation distribution is spatially heterogeneous, with some areas receiving as little as 46% of the incident radiation observed under no-panel conditions.
- Shading–Water Interaction: Moderate shading can reduce evapotranspiration enough to improve biomass accumulation in specific zones, even surpassing unshaded yields by up to 10 %.
- Land-Use Synergy: Elevating PV modules at 3 m and spacing rows 5 m apart allows standard cultivation practices, though a total 12% yield reduction per hectare occurs.
- Design Sensitivity: Panel tilt angle, clearance, and row spacing critically affect the spatial pattern of shade, underlining the need for site-specific optimization to minimize yield penalties.

NOMENCLATURE

Symbols		
B(t)	Cumulative biomass at day t	(g/m^2)
β	Tilt angle of PV panels	(°)
DHI	Diffuse Horizontal Irradiance	(W/m^2)
fCO_2	CO_2 concentration stress factor	(–)
fheat	Heat–stress factor	(–)
fSolar	Fraction of incoming PAR intercepted by canopy	(–)
ftemp	Temperature–stress factor	(–)
fwater	Water–stress factor	(–)
GDD	Growing Degree-Day	(°Cday)
GHI	Global Horizontal Irradiance	(W/m^2)
h	Panel height above ground	(m)
HI	Harvest Index	(–)
I_{50A}	Thermal time for 50% light interception (growth phase)	(°Cday)
I_{50B}	Thermal time for 50% light interception (senescence)	(°Cday)
l	Module length	(m)
P	Precipitation	(mm)
PAR	Photosynthetically Active Radiation	(W/m^2)
RUE	Radiation Use Efficiency	(g/MJ)
RH	Relative Humidity	(%)
T	Air temperature	(°C)
T_{base}	Base temperature for biomass growth	(°C)
T_{mean}	Mean daily temperature	(°C)
T_{opt}	Optimal temperature for biomass growth	(°C)
T_{heat}	Heat stress threshold temperature	(°C)
T_{sum}	Cumulative GDD for physiological maturity	(°Cday)
u	Wind speed	(m/s)
w	Module width	(m)
γ_s	Sun's azimuth angle	(°)
θ_z	Sun's zenith angle	(°)
Acronyms		
AV	Agrivoltaic	
PV	Photovoltaic	

REFERENCES

1. Alibaba, 2023, "Solar Panel 2m × 1m Commercial Specifications," E-Commerce Listing, URL: https://www.alibaba.com/showroom/solar-panel-2m-x-1m.html (Accessed [10 Nov. 2024]).

2. Amaducci, S., Yin, X., Colauzzi, M., 2018, "Agrivoltaic systems to optimize land use for electric energy production" *Appl. Energy*, 220: p. 545–561.
3. Asseng, S., Foster I., Turner, C., 2011, "The impact of temperature variability on wheat yields" *Global Change Biology*, 17: p. 997–1012.
4. Badr, M.A., El-Thonamy W.A., Salman S.R., Gruda N., 2022, "Yield and water use relationships of potato under different timing and severity of water stress", *Agric. Water Manag*., 271: p. 107793.
5. Barron-Gafford, G.A., Pavao-Zuckerman, M.A., Minor, R.L., *et al*., 2019, "Agrivoltaics provide mutual benefits across the food–energy–water nexus in drylands," *Nature Sustain*., 2: p. 848–855.
6. Elamri, S., Cheviron, B., Lopez, J.-M., *et al.*, 2018, "Water budget and crop modelling for agrivoltaic systems: application to irrigated lettuces," *Agric. Water Manag*., 208: p. 440–453.
7. European Commission, Joint Research Centre, 2023, "Photovoltaic Geographical Information System (PVGIS)," Online Database, URL: https://joint-research-centre.ec.europa.eu/photovoltaic-geographical-information-system-pvgis_en (Accessed [15 Dec. 2024]).
8. Ferrera-Cobos *et al*., 2020, "Analysis of Spatial and Temporal Variability of the PAR/GHI Ratio and PAR Modeling Based on Two Satellite Estimates", *Remote Sensing*, 12(8), p. 1262.
9. Foyo-Moreno, I., Alados, I., Alados-Arboledas, L., 2017, "A new empirical model to estimate hourly diffuse photosynthetic photon flux density", *Atmospheric Research*, 203, p. 189-196
10. Ingrao, C., Strippoli, R., Lagioia, G., Huisingh, D., 2023, "Water scarcity in agriculture: An overview of causes, impacts and approaches for reducing the risks" *Heliyon*, 9: p. e18507.
11. ISMEA, 2024 "News di mercato – ortaggi e patate" ISMEA, URL: chrome-extension://efaidnbmnnnibpcajpcglclefindmkaj/https://www.ismea.it/flex/files/D.900baca302cbcaf71ad9/news_mercati__14_speciale_patate.pdf (Accessed [10 Jan. 2025]).
12. Mamun, M, A., Dargusch, P., Wadley, D. *et al*., 2022, "A review of research on agrivoltaic systems" *Renew. And Sust. Energy Reviews*, 161: p. 112351.
13. McCree K.J., 1966, "A solarimeter for measuring photosynthetically active radiation", *Agricultural Meteorology*, 3, p. 353-366
14. Monteith 1965, "Light distribution and photosynthesis in field crops," *Ann. of Botany*, 29: p.17–37
15. Pulighe, G., Di Fonzo, A., Gaito, M. *et al*., 2024, "Climate change impact on yield and income of Italian agriculture system: a scoping review" *Agricultural and Food Economics*, 12.
16. Renewable Ninja, 2023, "Renewable Ninja Precipitation Data," Online Database, URL: https://www.renewables.ninja/ (Accessed [10 Jan. 2025]).
17. Ritchie, J.T., Godwin, D.C., Otter-Nacke, S., 1985. "*CERES-wheat: A User-oriented Wheat Yield Model. Preliminary Documentation*". AGRISTARS, YM-U3 04442-JSC-18892.
18. Ross, J., 1981, "*The Radiation Regime and Architecture of Plant Stands*", Dr. W. Junk Publishers, The Hague, 391 p.
19. Hsiao, T.C., Heng, L., Steduto, P., 2009, "AquaCrop—The FAO Crop Model to Simulate Yield Response to Water: III. Parametrization and Testing for Maize". *Agronomy Journal*, 101(3).
20. Tan, Y., Liu, J., Li, W. *et al.*, 2025, "Agrivoltaics development progresses: From the perspective of photovoltaic impact on crops, soil ecology and climate" *Environmental Research*, 266: p. 120540.
21. Tsubo, M., Walker, S., 2005, "Relationships between photosynthetically active radiation and clearness index at Bloemfontein, South Africa", *Theor. and Appl. Climatology*, 80, p. 17-25
22. Valle, B., Simonneau, T., Sourd, F., *et al.*, 2017 "Increasing the total productivity of a land by combining mobile photovoltaic panels and food crops", *Appl. Energy*, 206, p. 1495-1507
23. Waddington E., 2024. "*How To Grow The Highly Prized Desiree Potato, A Versatile Red-Skinned Cultivar*." Hortic. Mag., https://horticulture.co.uk/potatoes/desiree/. (Accessed: [12 Oct. 2024]).
24. Widmer, J., Christ, B., Grenz, J., Norgrove, L., 2024, "Agrivoltaics, a promising new tool for electricity and food production: A systematic review" *Ren. and Sust. Energy Rev*., 192: p. 114277
25. Weselek, A., Bauerle, A., *et al.*, 2021, "Agrivoltaic system impacts on microclimate and yield of different crops within an organic crop rotation in a temperate climate" *Agr. for Sust. Devel*, 41.
26. Woli, P., Jones, J., Ingram, K., Fraisse, C., 2012, "Agricultural reference index for drought (ARID)". *Agronomy Journal*, 104 (2), 287–300.
27. Zavalloni, M., D'Alberto, R., Raggi, M., Viaggi, D., 2021, "Farmland abandonment, public goods and the CAP in a marginal area of Italy" *Land Use Policy*, 107: p. 104365.
28. Zhao, C., *et al*., 2019, "A SIMPLE crop model", *European Journal of Agronomy*, 104, p. 97-106